DNA Polymerase as a Molecular Motor and Pump

Samudra Sengupta,[†] Michelle M. Spiering,[†] Krishna K. Dey,[†] Wentao Duan,[†] Debabrata Patra,[†] Peter J. Butler,[‡,*] R. Dean Astumian,[§,*] Stephen J. Benkovic,[†,*] and Ayusman Sen[†,*]

[†]Department of Chemistry and [‡]Department of Bioengineering, The Pennsylvania State University, University Park, Pennsylvania 16802, United States, and [§]Department of Physics and Astronomy, The University of Maine, Orono, Maine 04469, United States

ABSTRACT

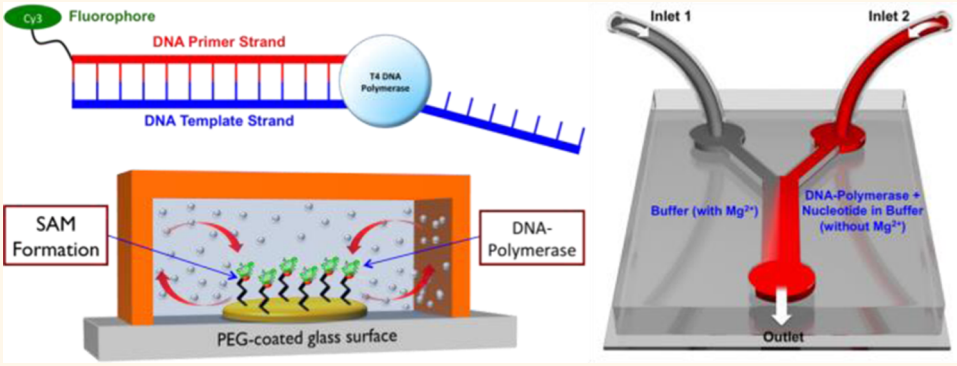

DNA polymerase is responsible for synthesizing DNA, a key component in the running of biological machinery. Using fluorescence correlation spectroscopy, we demonstrate that the diffusive movement of a molecular complex of DNA template and DNA polymerase enhances during nucleotide incorporation into the growing DNA template. The diffusion coefficient of the complex also shows a strong dependence on its inorganic cofactor, Mg^{2+} ions. When exposed to gradients of either nucleotide or cofactor concentrations, an ensemble of DNA polymerase complex molecules shows collective movement toward regions of higher concentrations. By immobilizing the molecular complex on a patterned gold surface, we demonstrate the fabrication of DNA polymerase-powered fluid pumps. These miniature pumps are capable of transporting fluid and tracer particles in a directional manner with the pumping speed increasing in the presence of the cofactor. The role of DNA polymerase as a micropump opens up avenues for designing miniature fluid pumps using enzymes as engines.

KEYWORDS: enzyme · DNA polymerase · catalysis · diffusion · nanomotor · chemotaxis · pump

Propulsion of objects at the nano- and microscale can be achieved by utilizing the chemical free energy of the surrounding medium.[1−13] In most cases, the energy is derived by catalytic turnover of a fuel or substrate in the vicinity of the motor to generate mechanical work for performing useful functions.[1−13] In particular, there has been significant interest in developing catalytic motors because the ability to rationally design synthetic and hybrid nano/micromotor systems will facilitate the emergence of novel smart devices. Upon immobilization, these catalytic motors can also impart their energy to the surrounding fluid. Using this concept, a number of artificial micropumps have been designed, which are capable of driving both fluid and small particles alike.[14−31]

The major inspiration behind designing artificial nano/micromotors and micropumps is to mimic the precision and efficiency of the naturally occurring biomotors like kinesins, myosins, and dyneins. Enzyme-driven biological motors are responsible for driving the biased motion of organisms in response to specific stimuli (chemicals or light).[32−36] Due to their vast diversity, enzyme-based artificial motors become an obvious choice for the next generation of intelligent devices that may enable nanotechnological and medical applications, such as dynamic self-assembly of superstructures, drug delivery, and lab-on-a-chip devices.[2−4,10,11] Recently, we have reported a substrate-concentration-dependent increase in diffusion of both catalase and urease in the presence of their respective

* Address correspondence to pbutler@psu.edu, astumian@maine.edu, sjb1@psu.edu, asen@psu.edu.

Received for review November 18, 2013 and accepted February 27, 2014.

Published online March 06, 2014
10.1021/nn405963x

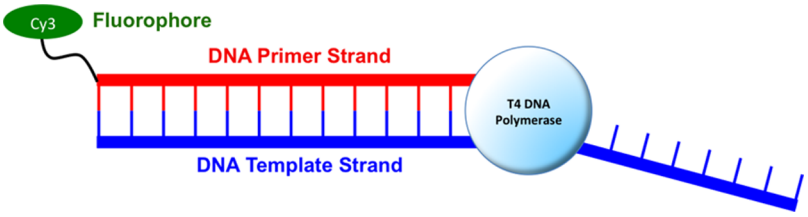

Figure 1. Schematic overview showing nucleotide incorporation on a DNA template by a DNA polymerase motor.

substrates, hydrogen peroxide and urea.[37,38] These enzyme molecules can also sense a gradient in substrate concentration and exhibit collective migration toward a higher substrate concentration. Schwartz and co-workers also reported a similar behavior with T7 RNA polymerase.[39]

Biological motors perform specific functions in living systems.[40−42] The T4 DNA polymerase is a well-characterized biomotor that is responsible for the sequential incorporation of nucleotides to synthesize DNA (Figure 1).[40] The polymerase adds deoxynucleotide triphosphates (dNTP) to the growing DNA strand, and the energy released from the removal of the pyrophosphate group results in the formation of a phosphoester bond that covalently links the deoxynucleotide monophosphate (dNMP) to the growing DNA chain. The polymerase motor binds to the DNA template inducing an internal conformational change in the polymerase.

The wild-type DNA polymerase has two active sites—the polymerase site that incorporates bases with high precision, and the exonuclease site, which acts as an error correction site to remove any mismatched nucleotides incorporated in the DNA primer strand. The motor can switch the DNA primer strand from the polymerase site to the exonuclease site whenever a mismatched nucleotide is identified and, after the error correction, rapidly revert the DNA strand back to the polymerase site for the replication process to continue.

In the presence of an excess of the single nucleotide templated next for incorporation, the polymerase is restricted to an idling state. During the idling−turnover process, the protein switches the DNA primer strand back and forth between the polymerase and the exonuclease active sites, incorporating and removing the nucleotide, thereby converting dNTP to dNMP until the nucleotide is completely depleted. With an exonuclease site mutant of DNA polymerase (exo-), a single nucleotide is incorporated, but subsequent cycles of incorporation and removal are prohibited. Both the polymerase site and the exonuclease site require the inorganic cofactor of two Mg^{2+} ions per site for activity. These unique functions of the DNA polymerase encouraged us to explore its possible role as a nanomotor outside biological systems and to investigate its further potential as a micropump when immobilized onto a surface.

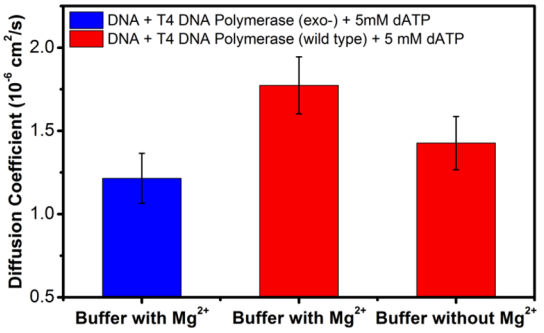

Figure 2. Diffusion studies of the DNA polymerase molecular complex. The diffusion coefficient of the wild-type polymerase DNA molecular complex in the idling−turnover mode showed an increase of 46% in the presence of 5 mM dATP (substrate nucleotide) and Mg^{2+} ions (cofactor) in the buffer over the diffusion coefficient of the DNA polymerase (exo-) complex. The increase in the diffusion coefficient of the molecular complex was lowered in the absence of Mg^{2+} ions in the buffer. The three diffusion coefficients are significantly different from each other with a significance value of $P < 0.015$. Error bars represent standard deviations. The means and standard deviations were calculated for 10 different measurements.

In this study, we show that the diffusive movement of a molecular complex of DNA template and T4 DNA polymerase is enhanced in the presence of a nucleotide, 2′-adenosine triphosphate (dATP). The molecular complex shows a collective directional movement in the presence of a dATP concentration gradient. Further, in the presence of a concentration gradient of the Mg^{2+} cofactor, it migrates toward areas of higher Mg^{2+} concentration. Finally, by immobilizing the molecular complex on a patterned surface, fluid and tracer particles can be pumped in a directional manner with the pumping speed increasing in the presence of cofactor in the surrounding fluid.

RESULTS AND DISCUSSION

The diffusive mobility of a wild-type T4 DNA polymerase complexed with DNA was measured in the presence of a substrate nucleotide in an idling−turnover mode. We used fluorescence correlation spectroscopy (FCS), an ultrasensitive technique, for diffusion studies.[43,44] The primer strand of the DNA was labeled with a fluorescent tag for monitoring by FCS. Diffusion of the DNA polymerase (exo-) complex was monitored as a control (Figure 2). The measured diffusion coefficient of the complex was 1.22×10^{-6} cm^2/s. The diffusion coefficient of the wild-type

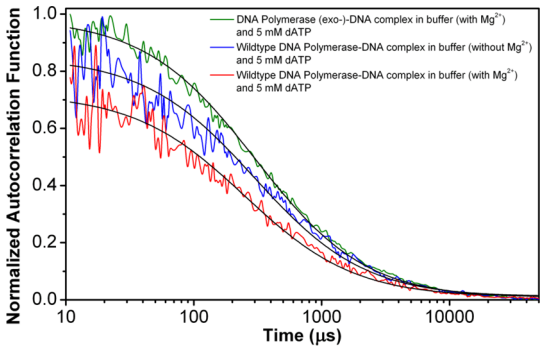

Figure 3. Fluorescence correlation spectroscopy traces. FCS traces for DNA polymerase complex molecules showing a plot of the normalized autocorrelation as a function of time. The traces shown are for wild-type polymerase DNA complexes in buffer with and without Mg^{2+} ions in the presence of 5 mM dATP (red and blue, respectively) and polymerase (exo-) DNA complexes in buffer with Mg^{2+} ions in the presence of 5 mM dATP (green).

polymerase DNA complex increased to 1.77×10^{-6} cm^2/s in the presence of 5 mM dATP in buffer with Mg^{2+}, a 46% increase in diffusion (Figure 2). This increase in diffusion was attenuated in the absence of Mg^{2+} in the buffer (Figure 2). The slight increase in diffusion of the complex molecules in the absence of cofactor can be attributed to some residual or contaminant Mg^{2+} ions present in the buffer in which the protein was stored. FCS traces for a wild-type polymerase DNA molecular complex in buffer (with and without Mg^{2+} ions) in the presence of 5 mM dATP (red and blue, respectively) and DNA polymerase (exo-) molecular complex in buffer (with Mg^{2+} ions) in the presence of 5 mM dATP (green) are shown in Figure 3. A shift in the FCS trace to the left corresponds to a faster diffusion rate.

We studied the collective migration behavior of the molecular complex in the presence of a dATP concentration gradient. We utilized a three-inlet microfluidic device (see Supporting Information, Figure S1A) to generate a dATP substrate nucleotide gradient. DNA in buffer with Mg^{2+} was injected through the center inlet, flanked by DNA polymerase and 10 mM dATP in buffer with Mg^{2+} on one side and buffer with Mg^{2+} on the other. As a control, the DNA was injected through the center inlet, flanked by DNA polymerase in buffer with Mg^{2+} through one side inlet and buffer with Mg^{2+} through the other side inlet. Using a syringe pump, a linear laminar flow rate of 1.85×10^4 μm/s was maintained in the main channel. The collective spreading behavior was studied using a fluorescence imaging setup. Lateral fluorescent spreading of the polymerase DNA complex was measured across the channel 40 mm downstream in the main channel. The fluorescence intensity profiles were normalized between 0 (minimum) and 1 (maximum) to quantify the shift at a defined value of fluorescence intensity. We observed that the normalized fluorescent intensity profile of the molecular complex showed a lateral spreading of 9 μm toward the substrate nucleotide in the presence of dATP as compared to no substrate (Figure 4A). Broadening of the fluorescence intensity profile was observed in the non-normalized plots in the presence of dATP as compared with no nucleotide, which is a direct consequence of the collective migration behavior (Supporting Information, Figure S2B); a similar effect was observed with urease and catalase.[37] As expected, a smaller shift in the normalized fluorescence intensity profile of 4.5 μm was observed when the laminar flow rate was doubled to 3.70×10^4 μm/s (Figure 4B). The non-normalized plots once again showed the anticipated broadening of the fluorescence intensity profile (see Supporting Information, Figure S2).

Further, we explored the response of the polymerase DNA complex to a concentration gradient of its cofactor, Mg^{2+} ions. As discussed before, a fluorescence imaging setup was utilized for studying the spreading behavior, and a two-inlet microfluidic channel (see Supporting Information, Figure S1B) was used for generating a Mg^{2+} ion concentration gradient. A mixture of polymerase DNA complex, 10 mM dATP, and buffer without Mg^{2+} ions was injected through one of the inlets, and buffer with 20 mM Mg^{2+} ions was injected through the other inlet. A lateral shift in the fluorescence intensity profile of 9 μm toward the region with the cofactor as compared to no Mg^{2+} ions was observed 40 mm down the channel (Figure 5).

On the basis of the observed enhanced diffusion of polymerase DNA complex in the presence of dATP, we hypothesized that the complex when immobilized on a surface should create flow in the surrounding fluid due to symmetry breaking. Accordingly, a circular gold pattern was designed on a PEG-coated glass surface using an e-beam evaporator. Utilizing Au−thiol chemistry, a quaternary ammonium-terminated ligand (see Supporting Information, Figure S3 and Scheme S1) was functionalized onto the Au pattern. The ligand formed a self-assembled monolayer (SAM) on the gold surface. The negatively charged backbone of the DNA bound selectively to the SAM-functionalized gold surface *via* electrostatic interactions. The DNA polymerase forms a complex with the DNA bound to the gold surface (Figure 6). The selective functionalization of the DNA polymerase complex on the SAM-modified Au pattern was verified by incubating the surface with fluorescent-labeled DNA. Then the surface was monitored under a fluorescence microscope. Fluorescence signal was observed only on the Au pattern, confirming the presence of DNA on the Au pattern (see Supporting Information, Figure S4). No fluorescence intensity was detected on the PEG-coated glass surface. To demonstrate the pumping ability of immobilized enzymes, a spacer was placed on top of the enzyme-patterned surface. Sulfate-functionalized polystyrene beads

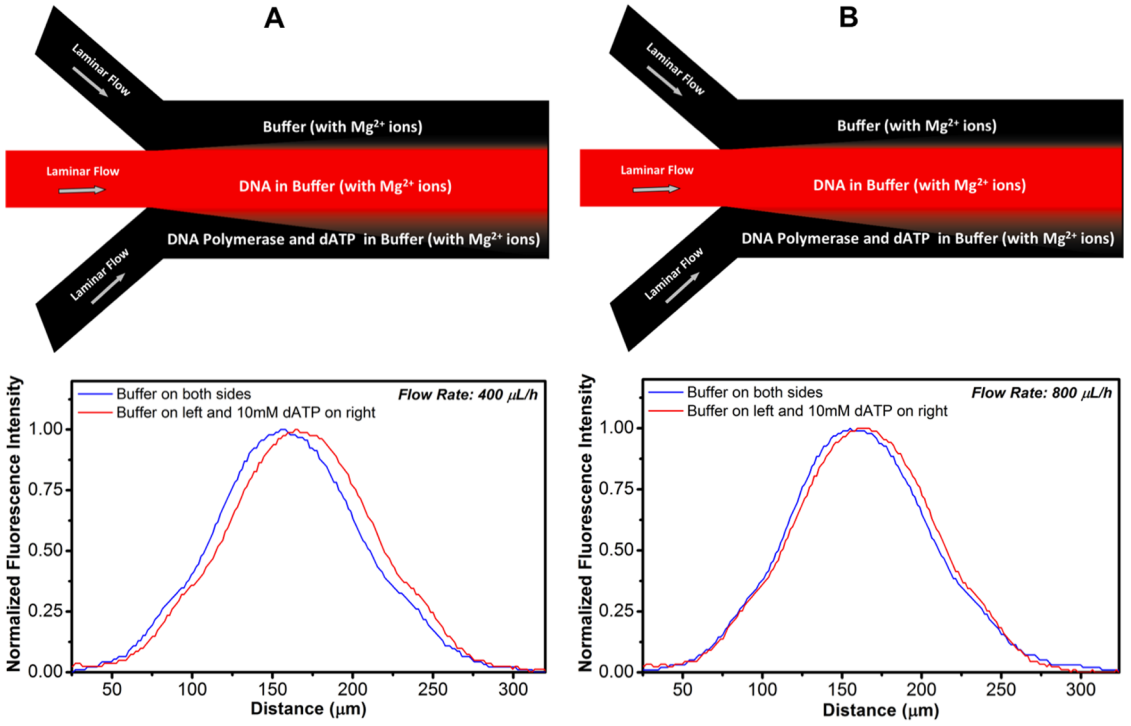

Figure 4. Collective migration of an ensemble of DNA polymerase complex molecules in response to a concentration gradient of substrate nucleotide. (A) Plot of mean normalized (1 corresponds to the maximum, and 0 corresponds to the minimum) fluorescence intensity (a.u.) profile as a function of the lateral position along the width of the channel shows a ~9 μm shift for an ensemble of DNA polymerase molecular complex toward 10 mM dATP (red; right side of the plot) as compared to buffer with Mg^{2+} ions (blue; right side of the plot) when viewed 40 mm down the channel and at a flow rate of 400 μL/h. The shift in the plot (red) to the right corresponds to a shift toward the dATP channel. (B) Plot of mean normalized fluorescence intensity (a.u.) profile as a function of the lateral position along the width of the channel shows a ~4.5 μm shift for an ensemble of DNA polymerase molecular complex toward 10 mM dATP (red; right side of the plot) as compared to buffer with Mg^{2+} ions (blue; right side of the plot) when viewed 40 mm down the channel and at a flow rate of 800 μL/h. The shift in the plot (red) to the right corresponds to a shift toward the dATP channel.

suspended in a buffered solution of dATP with Mg^{2+} ions were used as tracers to monitor the fluid flow. In the presence of 10 mM dATP in buffer with Mg^{2+}, the tracer particles moved in toward the gold surface at an average speed of 1.4 μm/s (Figure 7; see Supporting Information, video 1). When the concentration of dATP was lowered to 1 mM, the average fluid pumping speed decreased to 1.0 μm/s (Figure 7). However, in the absence of Mg^{2+} ions in the buffer, reduced fluid pump speeds of 0.4 μm/s were observed both in 10 mM dATP and 1 mM dATP (Figure 7; see Supporting Information, video 2). No fluid pumping was detected in the absence of the dATP substrate (see Supporting Information, video 3). Since the micropump design utilized here is a closed system, fluid flowing toward the Au disk near the PEG-coated glass surface should flow away from it in another plane by fluid continuity. Indeed, the fluid was found to flow away from the gold surface in another plane.

We considered a number of possibilities for the observed increase in diffusivity of the polymerase DNA molecular motor. The presence of substrate had a negligible effect on the solvent viscosity. The viscosity of buffer containing either 5 or 10 mM dATP was not significantly different. Bulk rise in solution temperature due to enzymatic catalysis of urea and hydrogen peroxide by urease and catalase, respectively, has been estimated and reported to be in the micro-Kelvin range.[37,38] Similarly, the possibility of a rise in solution temperature due to nucleotide incorporation in the DNA was estimated and found to be too small to account for the observed increase in diffusion (see Supporting Information). Active transport of catalytic particles in fluids can be achieved by various local and global force fields.[1−13,45−54] Recently, enhancement in diffusion of single-molecule urease, catalase, and RNA polymerase enzymes in the presence of their respective substrates has been reported.[37−39] The observed increase in diffusion occurred irrespective of the charge on the reaction products (neutral or ionic). Incorporation of a nucleotide into the DNA by the polymerase is accompanied by the release of pyrophosphate, the release of which can drive the molecular complex by a self-electrophoretic mechanism.[47,53] However, such a mechanism is unlikely to play a prominent role due to the very fast rotational diffusion of the DNA polymerase complex, which will normalize any concentration gradient of pyrophosphate generated in the vicinity of the complex.

An alternative explanation for the enhanced diffusion is based on a cycle of nonreciprocal conformational

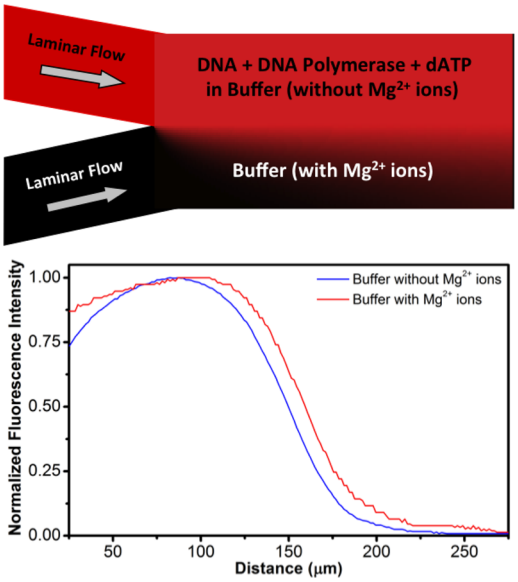

Figure 5. Collective migration of an ensemble of DNA polymerase complex molecules in response to a concentration gradient of cofactor. A plot of mean normalized (1 corresponds to the maximum, and 0 corresponds to the minimum) fluorescence intensity profile (a.u.) as a function of the lateral position along the width of the channel shows a ~9 μm shift for an ensemble of DNA polymerase molecules toward buffer with 20 mM Mg^{2+} ions (red) as compared to buffer with no Mg^{2+} ions (blue) when viewed 40 mm down the channel.

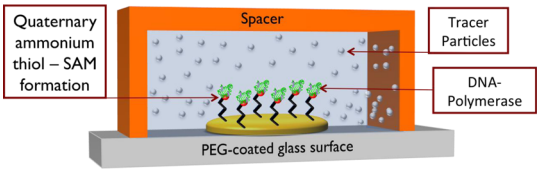

Figure 6. Schematic of a DNA polymerase-powered micropump. Au is patterned on a PEG-coated glass surface. The patterned surface is functionalized with a quaternary ammonium thiol, which forms a SAM (self-assembled monolayer) on the Au surface. The negatively charged backbone of the DNA binds selectively to the SAM-functionalized Au-patterned surface *via* electrostatic interactions. The DNA polymerase forms a complex with the DNA bound to the gold surface. The schematic is not drawn to scale.

changes.[55] It has been proposed that enzymes can propel themselves in solution during catalytic turnover by going through a sequence of nonreciprocal conformational changes that encompass substrate binding and product release.[56−59] During the nucleotide incorporation process, DNA polymerase molecules go through a series of conformational steps which are well-documented.[60−63] It is possible that a cycle of asymmetric conformational changes can overcome random Brownian diffusion to cause autonomous motion of the molecular complex. During idling−turnover of the DNA polymerase motor, the repetitive incorporation of dATP molecules and their subsequent removal from the DNA template also involves a cycle of nonreciprocal conformational changes.

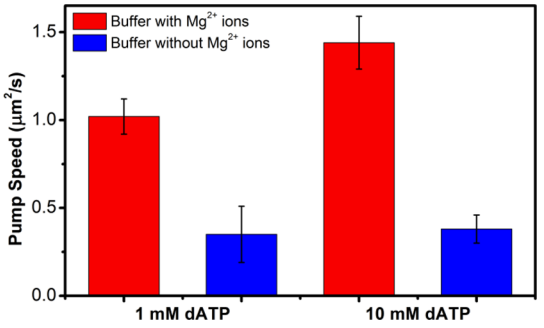

Figure 7. Fluid pumping in a DNA polymerase complex-powered micropump. The pumping speed of a DNA polymerase complex-powered pump increased with increasing the dATP concentration from 1 to 10 mM in the presence of Mg^{2+} ions. Fluid pumping is highly attenuated in the absence of Mg^{2+} ions. No fluid pumping was detected in the absence of dATP. Error bars represent standard deviations. The means and standard deviations are calculated for 30 tracer particles. The pumping velocities at different dATP concentrations and in the presence and absence of Mg^{2+} are statistically different ($P < 0.01$).

We propose that the collective spreading of an ensemble of molecular complexes toward higher substrate concentration results from an enhanced diffusion mechanism.[37,39,64,65] As the flows of DNA in the center inlet and polymerase/dATP in one of the side inlets diffuse into each other under laminar flow conditions, the polymerase binds to the DNA to form a molecular complex (dissociation constant of the molecular complex, K_D = 70 nM[66]). As the molecular complex moves across the channel, it encounters a higher nucleotide concentration and experiences a higher diffusion coefficient, which results in a greater spreading of the complex molecules toward higher nucleotide concentration. This is analogous to the substrate concentration gradient acting like a Brownian ratchet.[67−70] As an effect of this collective migration, the broadening of fluorescence intensity profiles was observed in the non-normalized plots (Supporting Information, Figure S2). Collective movement in a chemical gradient, an exceptional phenomenon outside biological systems, has been reported for ensembles of urease, catalase, and RNA polymerase enzymes.[37−39,54,64,65] We propose a similar mechanism, which is stochastic in nature, for the directional spreading behavior of the DNA polymerase complex toward higher Mg^{2+} cofactor concentration. The spreading behavior of the molecular complex observed in our experiments is different from biological chemotaxis as shown by bacteria, which requires temporal memory of the concentration gradient of their food.

An equally intriguing observation is the fluid pumping action exhibited by these molecular complexes when immobilized on a patterned surface. It was shown previously that catalysts supported on a surface can generate fluid pumping through catalytic turnover,[21−27,30,71] resulting from phoretic mechanisms such as diffusiophoresis,[45] osmophoresis,[54] and

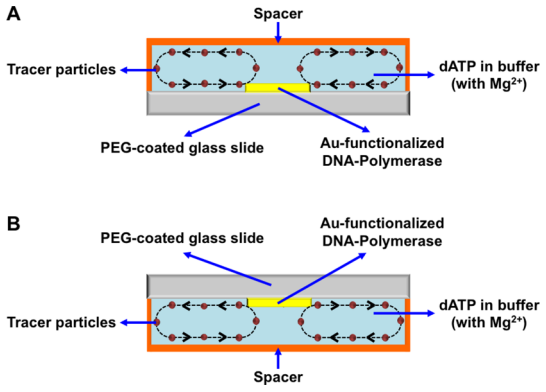

Figure 8. Fluid pumping in upright and inverted micropump setups. The direction of fluid flow monitored with both positive and negative tracers reverses direction relative to the glass surface when the pump setup is inverted (B) as compared to an upright setup (A). The fluid flow switches direction relative to the glass surface in the upright and inverted micropump setups due to a density-driven mechanism.

self-electrophoresis.[53] Transport of fluid and tracers in DNA polymerase-powered pumps may arise from an electrolyte diffusiophoretic mechanism since nucleotide incorporation into the DNA generates charged reaction products due to dATP hydrolysis.[46,72] The zeta-potential of tracer particles determines the direction of transport in electrolyte diffusiophoresis, with tracers with opposite charges moving in opposite directions. However, we observed that the direction of movement of positively charged amine-functionalized tracers was exactly the same as their negative sulfate-functionalized counterparts (see Supporting Information, video 4).

The fluid flow monitored with both positive and negative tracers reverses direction relative to the glass surface when the pump setup is inverted (Figure 8; also see Supporting Information, video 5). This is possible only when the flow is driven by a difference in density. Importantly, the energy released per second in the polymerase reaction is estimated to be nearly 10^{-9} W, while that required to drive fluid convection of the order of 1 μm/s (observed magnitude of flow) within the experimental chamber is nearly 10^{-16} W (see Supporting Information). The chemical energy available in the system is therefore more than sufficient to power the observed convective movement of the fluid. However, the mechanism by which the density gradient is established remains an open question. To estimate the role of reaction exothermicity, multiphysics simulations were performed in COMSOL, coupling the physics of heat transfer and laminar flow of liquid (see Supporting Information for details). The simulations confirmed that, in order to establish a convective flow of the order of 1 μm/s through a *purely thermal gradient*, the system needs to have a power input of approximately 10^{-4} W, which is far larger than the energy released in the polymerase reaction. Thus, we conclude that the density gradient and accompanying fluid convection generated in the present system are *nonthermal* in origin, suggesting the possibility that the observed phenomena may be due to nonreciprocal conformational changes occurring at the immobilized enzymes. This is reminiscent of the direct conversion of metabolic energy to kinetic energy that is responsible for fluid motion observed in the presence of free swimming bacteria.[73] The driven conformational changes of the polymerase molecules may increase the mean free path between water molecules near the surface, effectively reducing the density at that position. Alternatively, the conversion of dATP to dAMP + PPi may result in a net decrease in fluid density near the pump surface.[71] Either one of these proposed mechanisms is consistent with our experimental observations. In the upright setup in which the polymerase pattern is at the bottom, the fluid flow is directed upward from the pump, and near the bottom glass surface, the flow is toward the Au pattern due to fluid continuity. In the inverted setup where the pattern is at top of the device, the fluid flow is reversed because the less dense fluid prefers to occupy the upper layers and spreads along the glass surface away from the polymerase pattern. The observed energy conversion efficiency of the micropump ($\sim 10^{-7}$) is comparable to that of previously reported synthetic autonomous systems that also transduce the energy from chemical reactions to mechanical motion.[74,75]

ATP powers most of the biological pumps found in nature. While artificial micropumps have been designed,[15,76] this is the first example of a polymerase-powered pump. This pump has the unique capability to sense and respond to specific triggers: dATP and Mg^{2+} ions. The ability of enzymes and biomotors to pump fluids, small molecules, and particles in a directed fashion may enable the development of smart micro- and nanoscale devices that turn on in response to specific analytes and contain sophisticated levels of control over the location and flow rate of fluids.

CONCLUSION

In conclusion, we show that the incorporation of nucleotides into a DNA template by DNA polymerase is responsible for an enhancement in diffusion of the complex. It is possible that nonreciprocal conformational changes in this biomolecular complex play a role in the observed increase in diffusive mobility. Furthermore, in the presence of substrate and cofactor concentration gradients, an ensemble of these complexes spreads toward areas of higher concentration, which is a direct consequence of the enhanced diffusion exhibited by these complex molecules. Finally, by immobilizing DNA polymerase complexes on a patterned surface, fluid pumps can be designed and fabricated. The findings reported in this paper can be a stepping stone in the design of novel bioinspired motors and

micropumps that will have a wide range of applications from nano- and microscale sensing devices to cargo delivery vehicles. It has also not escaped our notice that the mechanisms of directed motion, enhanced diffusion and pumping, possibly due to nonreciprocal conformational changes, are generic and may play a fundamental role in biological motility and transport by biomolecular machines.

METHODS

Preparation of Fluorescent-Tagged DNA Sample. Fluorescent-labeled DNA primer oligomer (M_W = 4402.2, T_M = 53.8 °C, 100 nmol, HPLC purified, 5′-/5Cy3/TCG CAG CCG TCC A-3′) and DNA template oligomer (M_W = 6,127, T_M = 62.2 °C, 25 nmol, purified by standard desalting technique, 5′-AAA CCC TTG GAC GGC TGC GA-3′) were purchased from Integrated DNA Technologies. Using a UV−vis spectrophotometer, the concentrations of stock solutions of primer oligomer (ε = 122 100 M^{-1} cm^{-1}) and template oligomer (ε = 190 700 M^{-1} cm^{-1}) were measured as 56.92 and 91.61 μM, respectively. The absorbance was recorded at 260 nm at a path length of 1 cm. From the stock solutions, 10 μM solutions of both primer and template oligomers were prepared in 10 mM Tris, pH 8.0 buffer. The mixture was incubated at 65 °C in a water bath for 3 min and allowed to cool slowly to room temperature. The resulting fluorescent-tagged DNA sample was stored in aliquots of 50 μL at −20 °C. Wild-type T4 DNA polymerase was purified as previously described[77] and stored at −80 °C. Both the DNA and DNA polymerase samples were thawed on ice before experiments were performed.

Single-Molecule Diffusion Measurements with Fluorescence Correlation Spectroscopy (FCS). See Supporting Information for detailed FCS measurement conditions.

Microfluidic Device Fabrication. The microfluidic device was cast in polydimethylsiloxane (PDMS, Sylgard 184, Dow Corning) using standard soft lithography protocols.[78] A 100 μm deep master pattern, which contains the inverse-shaped microfluidic device, was created on a silicon wafer (Silicon Quest) by spin coating a thin layer of positive photoresist, SPR-220 resist (Microposit). The wafer containing the photoresist was treated and structured by using photolithography methods. This was followed by deep reactive ion etching (DRIE, Alcatel Speeder 100 deep silicon reactive ion etch) to generate the master stamp. The master silicon wafer was exposed to 1*H*,1*H*,2*H*,2*H*-perfluorooctyltrichlorosilane (Sigma Aldrich) in a vacuum desiccator to minimize adhesion of PDMS to the wafer during the peeling step. The PDMS was prepared by thoroughly mixing the PDMS base polymer and the curing agent in a 10:1 (weight/weight) ratio. The mixture was then degassed in a desiccator for about an hour and baked at 60 °C in an oven for 30 min. The PDMS was then cooled and peeled off. Pinholes acting as inlets and outlets were drilled open with a drill press (Dremel Model 220 WorkStation), a rotary tool (Dremel 300 Series), and drill bits (Drill Bit City). To ensure permanent bonding between the PDMS and the glass substrate, the device was sealed to a No. 1 glass coverslip (VWR) with a high-frequency generator (model BD-10AS, Electro-Technic Products, Inc.). Polyethylene tubing (Becton Dickinson and Company) was inserted into the inlets and outlet of the microfluidic device. Fluid flow through the microchannel was generated by syringe pumps (KDS 200 and 220, KD Scientific).

Fluorescence Imaging Setup. Collective migration of DNA polymerase complex molecules in the presence of a dATP concentration gradient was characterized using fluorescence imaging. The optical setup comprised an inverted microscope (Zeiss Axiovert 200 MAT) with a halogen lamp (12 V max, 100 W). Excitation light was passed through the appropriate filter cube (Zeiss) depending on the excitation/emission wavelengths of the fluorescent tag. It was then focused on to the sample through a 20× objective (EC Epiplan-NEOFLUAR 20×/0.5 HD DIC ∞/0, Zeiss). Fluorescence emission was collected by the objective, passed through interference filters, and finally detected by a high-sensitivity Flea 3 CCD camera (FL3-U3-32S2C-CS, Point Grey) with a resolution of 2080 × 1552 pixels at 60 frames per second.

Videos were recorded and analyzed using Image J software. In each experiment, the mean fluorescence intensity was calculated from a collection of 2500−3000 images. A region of interest (ROI) was selected along the channel, and the stack-averaged fluorescence intensity was plotted as a function of the width of the channel.

Lateral shifts in normalized fluorescence intensity were calculated as follows.

Two-Inlet Microfluidic Device. The central pixel was selected inside the ROI, and its normalized fluorescence intensity was measured in the absence of substrate. Then, in the presence of Mg^{2+} cofactor ions, the ROI was investigated again to find a pixel with an equivalent fluorescence intensity to the one previously measured. The lateral distance of this new pixel from the center of the channel was taken to be the lateral shift. The central pixel was chosen to calculate the lateral shifts in our measurements because the DNA polymerase molecules will experience the maximum gradient in cofactor concentration at this point.

Three-Inlet Microfluidic Device. A pixel was selected inside the ROI, which was midpoint between the DNA polymerase flow region and the substrate nucleotide flow region, and its normalized fluorescence intensity was measured in the absence of substrate. Then, in the presence of 10 mM dATP substrate, the ROI was investigated again to find a pixel with an equivalent fluorescence intensity to the one previously measured. The lateral distance of this new pixel from the one measured in the absence of substrate was taken to be the lateral shift. The pixel midpoint between the polymerase flow region and the nucleotide flow region was chosen to calculate the lateral shifts in our measurements because the DNA polymerase molecules will experience the maximum gradient in nucleotide concentration at this point.

Micropump Design, DNA Polymerase Immobilization, and Particle Tracking. Using an e-beam evaporator, Au was patterned on a PEG-coated glass surface (MicroSurfaces). The surface was cleaned thoroughly with isopropyl alcohol followed by acetone and dried under a nitrogen stream. Previously synthesized quaternary ammonium thiol[79] was used for self-assembled monolayer formation on the Au surface. The ligand was dissolved in a methanol/water mixture, and the surface was incubated in it overnight at room temperature under an inert atmosphere. Later, the surface was washed several times with a methanol mixture and dried under an inert atmosphere. The SAM-modified surface was incubated with a DNA solution for 4−5 h. The negatively charged backbone of the DNA molecules bound selectively to the Au-patterned surface *via* electrostatic interactions. The DNA polymerase forms a complex with the DNA molecules bound to the Au surface.

To monitor the fluid flow, functionalized polystyrene microspheres (2 μm) were introduced as tracers in our experiments. Videos were captured using an optical setup, which comprised a microscope (Olympus BX60M) with a halogen lamp (100 W) and a 50× objective lens (LMPlanFLN 50×/0.5 BD ∞/0/FN26.5, Olympus). Videos were recorded using a CCD camera attached to the optical microscope. For measuring fluid pumping speed, 30 particles were tracked using PhysVis software.

Conflict of Interest: The authors declare no competing financial interest.

Acknowledgment. We gratefully acknowledge financial support by the Penn State MRSEC under NSF Grant DMR-0820404 and, in part, by the Defense Threat Reduction Agency (HDTRA1-13-1-0039). This publication was also supported by the Pennsylvania State University Materials Research Institute

Nanofabrication Lab and the National Science Foundation Cooperative Agreement No. ECS-0335765.

Supporting Information Available: Single-molecule diffusion measurements with FCS, viscosity measurements, generation of nucleotide and cofactor concentration gradients, calculations for bulk temperature variations, synthesis of quaternary ammonium thiol ligand, supporting figures and supporting videos are provided. This material is available free of charge *via* the Internet at http://pubs.acs.org.

REFERENCES AND NOTES

1. Hong, Y.; Velegol, D.; Chaturvedi, N.; Sen, A. Biomimetic Behavior of Synthetic Particles: From Microscopic Randomness to Macroscopic Control. *Phys. Chem. Chem. Phys.* **2010**, *12*, 1423–1425.
2. Paxton, W. F.; Sundararajan, S.; Mallouk, T. E.; Sen, A. Chemical Locomotion. *Angew. Chem., Int. Ed.* **2006**, *45*, 5420–5429.
3. Sengupta, S.; Ibele, M. E.; Sen, A. Fantastic Voyage: Designing Self-Powered Nanorobots. *Angew. Chem., Int. Ed.* **2012**, *51*, 8434–8445.
4. Sanchez, S.; Pumera, M. Nanorobots: The Ultimate Wireless Self-Propelled Sensing and Actuating Devices. *Chem.—Asian J.* **2009**, *4*, 1402–1410.
5. Ozin, G. A.; Manners, I.; Fournier-Bidoz, S.; Arsenault, A. Dream Nanomachines. *Adv. Mater.* **2005**, *17*, 3011–3018.
6. Paxton, W. F.; Sen, A.; Mallouk, T. E. Motility of Catalytic Nanoparticles through Self-Generated Forces. *Chem.—Eur. J.* **2005**, *11*, 6462–6470.
7. Mei, Y.; Solovev, A. A.; Sanchez, S.; Schmidt, O. G. Rolled-up Nanotech on Polymers: From Basic Perception to Self-Propelled Catalytic Microengines. *Chem. Soc. Rev.* **2011**, *40*, 2109–2119.
8. Wang, J.; Manesh, K. M. Motion Control at the Nanoscale. *Small* **2010**, *6*, 338–345.
9. Mirkovic, T.; Zacharia, N. S.; Scholes, G. D.; Ozin, G. A. Nanolocomotion—Catalytic Nanomotors and Nanorotors. *Small* **2010**, *6*, 159–167.
10. Wang, J. Can Man-Made Nanomachines Compete with Nature Biomotors? *ACS Nano* **2009**, *3*, 4–9.
11. Patra, D.; Sengupta, S.; Duan, W.; Zhang, H.; Pavlick, R. A.; Sen, A. Intelligent, Self-Powered, Drug Delivery Systems. *Nanoscale* **2013**, *5*, 1273–1283.
12. Pumera, M. Nanomaterials Meet Microfluidics. *Chem. Commun.* **2011**, *47*, 5671–5680.
13. Mallouk, T. E.; Sen, A. Powering Nanorobots. *Sci. Am.* **2009**, *300*, 72–77.
14. Laser, D. J.; Santiago, J. G. A Review of Micropumps. *J. Micromech. Microeng.* **2004**, *14*, R35–R64.
15. Nisar, A.; Afzulpurkar, N.; Mahaisavariya, B.; Tuantranont, A. MEMS-Based Micropumps in Drug Delivery and Biomedical Applications. *Sens. Actuators, B* **2008**, *130*, 917–942.
16. Dash, A. K.; Cudworth, G. C., II. Therapeutic Applications of Implantable Drug Delivery Systems. *J. Pharmacol. Toxicol. Methods* **1998**, *40*, 1–12.
17. Jakeway, S. C.; de Mello, A. J.; Russell, E. L. Miniaturized Total Analysis Systems for Biological Analysis. *Fresenius J. Anal. Chem.* **2000**, *366*, 525–539.
18. van der Schoot, B.; Jeanneret, S.; van den Berg, A.; de Rooij, F. A. A Silicon Integrated Miniature Chemical Analysis System. *Sens. Actuators, B* **1992**, *6*, 57–60.
19. Khandurina, J.; McKnight, T. E.; Jacobson, S. C.; Waters, L. C.; Foote, R. S.; Ramsey, J. M. Integrated System for Rapid PCR-Based DNA Analysis in Microfluidic Devices. *Anal. Chem.* **2000**, *72*, 2995–3000.
20. Woolley, A. T.; Hadley, D.; Landre, P.; de Mello, A. J.; Mathies, R. A.; Northrup, M. A. Functional Integration of PCR Amplification and Capillary Electrophoresis in a Microfabricated DNA Analysis Device. *Anal. Chem.* **1996**, *68*, 4081–4086.
21. Zhang, H.; Yeung, K.; Robbins, J. S.; Pavlick, R. A.; Wu, M.; Liu, R.; Sen, A.; Phillips, S. T. Self-Powered Microscale Pumps Based on Analyte-Initiated Depolymerization Reactions. *Angew. Chem., Int. Ed.* **2012**, *51*, 2400–2404.
22. Kline, T. R.; Paxton, W. F.; Wang, Y.; Velegol, D.; Mallouk, T. E.; Sen, A. Catalytic Micropumps: Microscopic Convective Fluid Flow and Pattern Formation. *J. Am. Chem. Soc.* **2005**, *127*, 17150–17151.
23. Ibele, M. E.; Wang, Y.; Kline, T. R.; Mallouk, T. E.; Sen, A. Hydrazine Fuels for Bimetallic Catalytic Microfluidic Pumping. *J. Am. Chem. Soc.* **2007**, *129*, 7762–7763.
24. Jun, I. K.; Hess, H. A. A Biomimetic, Self-Pumping Membrane. *Adv. Mater.* **2010**, *22*, 4823–4825.
25. Hong, Y.; Diaz, M.; Córdova-Figueroa, U. M.; Sen, A. Light-Driven Titanium-Dioxide-Based Reversible Microfireworks and Micromotor/Micropump Systems. *Adv. Funct. Mater.* **2010**, *20*, 1568–1576.
26. Paxton, W. F.; Baker, P. T.; Kline, T. R.; Wang, Y.; Mallouk, T. E.; Sen, A. Catalytically Induced Electrokinetics for Motors and Micropumps. *J. Am. Chem. Soc.* **2006**, *128*, 14881–14888.
27. Solovev, A. A.; Sanchez, S.; Mei, Y.; Schmidt, O. G. Tunable Catalytic Tubular Micro-Pumps Operating at Low Concentrations of Hydrogen Peroxide. *Phys. Chem. Chem. Phys.* **2011**, *13*, 10131–10135.
28. Zhang, L.; Koo, J.-M.; Jiang, L.; Asheghi, M.; Goodson, K. E.; Santiago, J. G.; Kenny, T. W. Measurements and Modeling of Two-Phase Flow in Microchannels with Nearly Constant Heat Flux Boundary Conditions. *J. Microelectromech. Syst.* **2002**, *11*, 12–19.
29. Hogg, T.; Freitas, R. A. Chemical Power for Microscopic Robots in Capillaries. *Nanomedicine* **2010**, *6*, 298–317.
30. Yadav, V.; Zhang, H.; Pavlick, R. A.; Sen, A. Triggered "On/Off" Micropumps and Colloidal Photodiode. *J. Am. Chem. Soc.* **2012**, *134*, 15688–15691.
31. Andersson, H.; van der Wijngaart, W.; Nilsson, P.; Enoksson, P.; Stemme, G. A Valve-Less Diffuser Micropump for Microfuidic Analytical Systems. *Sens. Actuators, B* **2001**, *72*, 259–265.
32. Adler, J. Chemoreceptors in Bacteria. *Science* **1969**, *166*, 1588–1597.
33. Berg, H. C.; Brown, D. A. Chemotaxis in *Escherichia coli* Analysed by Three-Dimensional Tracking. *Nature* **1972**, *239*, 500–504.
34. van Haastert, P. J. M.; Devreotes, P. N. Chemotaxis: Signalling the Way Forward. *Nat. Rev. Mol. Cell Biol.* **2004**, *5*, 626–634.
35. Engelmann, T. W. Neue Methode zur Untersuchung der Sauerstoffausscheidung Pflanzlicher und Tierischer Organismen. *Pfluegers Arch. Gesamte Physiol. Menschen Tiere* **1881**, *25*, 285–292.
36. Engelmann, T. W. Zur Biologie der Schizomyceten. *Pfluegers Arch. Gesamte Physiol. Menschen Tiere* **1881**, *26*, 537–545.
37. Sengupta, S.; Dey, K. K.; Muddana, H. S.; Tabouillot, T.; Ibele, M. E.; Butler, P. J.; Sen, A. Enzyme Molecules as Nanomotors. *J. Am. Chem. Soc.* **2013**, *135*, 1406–1414.
38. Muddana, H. S.; Sengupta, S.; Mallouk, T. E.; Sen, A.; Butler, P. J. Substrate Catalysis Enhances Single Enzyme Diffusion. *J. Am. Chem. Soc.* **2010**, *132*, 2110–2111.
39. Yu, H.; Jo, K.; Kounovsky, K. L.; de Pablo, J. J.; Schwartz, D. C. Molecular Propulsion: Chemical Sensing and Chemotaxis of DNA Driven by RNA Polymerase. *J. Am. Chem. Soc.* **2009**, *131*, 5722–5723.
40. Goel, A.; Vogel, V. Harnessing Biological Motors To Engineer Systems for Nanoscale Transport and Assembly. *Nat. Nanotechnol.* **2008**, *3*, 465–475.
41. Lipowsky, R.; Beeg, J.; Dimova, R.; Klumpp, S.; Liepelt, S.; Müller, M. J. I.; Valleriani, A. Active Bio-Systems: from Single Motor Molecules to Cooperative Cargo Transport. *Biophys. Rev. Lett.* **2009**, *4*, 77–137.
42. Puchner, E. M.; Gaub, H. E. Single-Molecule Mechanoenzymatics. *Annu. Rev. Biophys.* **2012**, *41*, 497–518.
43. Gullapalli, R. R.; Tabouillot, T.; Mathura, R.; Dangaria, J. H.; Butler, P. J. Integrated Multimodal Microscopy, Time-Resolved Fluorescence, and Optical-Trap Rheometry: Toward Single Molecule Mechanobiology. *J. Biomed. Opt.* **2007**, *12*, 014012-1–014012-17.
44. Lakowicz, J. R. In *Principles of Fluorescence Spectroscopy*, 3rd ed.; Springer: New York, 2006.

45. Anderson, J. L.; Prieve, D. C. Diffusiophoresis: Migration of Colloidal Particles in Gradients of Solute Concentration. *Sep. Purif. Methods* **1984**, *13*, 67–103.
46. Anderson, J. L. Colloid Transport by Interfacial Forces. *Annu. Rev. Fluid Mech.* **1989**, *21*, 61–99.
47. Paxton, W. F.; Kistler, K. C.; Olmeda, C. C.; Sen, A.; St. Angelo, S. K.; Cao, Y.; Mallouk, T. E.; Lammert, P. E.; Crespi, V. H. Catalytic Nanomotors: Autonomous Movement of Striped Nanorods. *J. Am. Chem. Soc.* **2004**, *126*, 13424–13431.
48. Golestanian, R.; Liverpool, T. B.; Ajdari, A. Propulsion of a Molecular Machine by Asymmetric Distribution of Reaction Products. *Phys. Rev. Lett.* **2005**, *94*, 220801-1–220801-4.
49. Golestanian, R.; Liverpool, T. B.; Ajdari, A. Designing Phoretic Micro- and Nano-Swimmers. *New J. Phys.* **2007**, *9*, 126-1–126-8.
50. Howse, J. R.; Jones, R. A. L.; Ryan, A. J.; Gough, T.; Vafabakhsh, R.; Golestanian, R. Self-Motile Colloidal Particles: From Directed Propulsion to Random Walk. *Phys. Rev. Lett.* **2007**, *99*, 048102-1–048102-4.
51. Córdova-Figueroa, U. M.; Brady, J. F. Osmotic Propulsion: The Osmotic Motor. *Phys. Rev. Lett.* **2008**, *100*, 158303-1–158303-4.
52. Ke, H.; Ye, S.; Carroll, R. L.; Showalter, K. Motion Analysis of Self-Propelled Pt-Silica Particles in Hydrogen Peroxide Solutions. *J. Phys. Chem. A* **2010**, *114*, 5462–5467.
53. Moran, J. L.; Posner, J. D. Electrokinetic Locomotion Due to Reaction-Induced Charge Auto-Electrophoresis. *J. Fluid Mech.* **2011**, *680*, 31–66.
54. Pavlick, R. A.; Sengupta, S.; McFadden, T.; Zhang, H.; Sen, A. A Polymerization-Powered Motor. *Angew. Chem., Int. Ed.* **2011**, *50*, 9374–9377.
55. Purcell, E. M. Life at Low Reynolds Number. *Am. J. Phys.* **1977**, *45*, 3–11.
56. Sakaue, T.; Kapral, R.; Mikhailov, A. S. Nanoscale Swimmers: Hydrodynamic Interactions and Propulsion of Molecular Machines. *Eur. Phys. J. B* **2010**, *75*, 381–387.
57. Cressman, A.; Togashi, Y.; Mikhailov, A. S.; Kapral, R. Mesoscale Modeling of Molecular Machines: Cyclic Dynamics and Hydrodynamical Fluctuations. *Phys. Rev. E* **2008**, *77*, 050901-1–050901-4.
58. Golestanian, R. Synthetic Mechanochemical Molecular Swimmer. *Phys. Rev. Lett.* **2010**, *105*, 018103-1–018103-4.
59. Golestanian, R.; Ajdari, A. Mechanical Response of a Small Swimmer Driven by Conformational Transitions. *Phys. Rev. Lett.* **2008**, *100*, 038101-1–038101-4.
60. Johnson, K. A. Conformation Coupling in DNA Polymerase Fidelity. *Annu. Rev. Biochem.* **1993**, *62*, 685–713.
61. Franklin, M. C.; Wang, J.; Steitz, T. A. Structure of the Replicating Complex of a Pol Alpha Family DNA Polymerase. *Cell* **2001**, *105*, 657–667.
62. Shamoo, Y.; Steitz, T. A. Building a Replisome from Interacting Pieces: Sliding Clamp Complexed to a Peptide from DNA Polymerase and a Polymerase Editing Complex. *Cell* **1999**, *99*, 155–166.
63. Wang, J.; Sattar, A. K.; Wang, C. C.; Karam, J. D.; Konigsberg, W. H.; Steitz, T. A. Crystal Structure of a Pol Alpha Family Replication DNA Polymerase from Bacteriophage RB69. *Cell* **1997**, *89*, 1087–1099.
64. Hong, Y.; Blackman, N. M. K.; Kopp, N. D.; Sen, A.; Velegol, D. Chemotaxis of Nonbiological Colloidal Rods. *Phys. Rev. Lett.* **2007**, *99*, 178103-1–178103-4.
65. Baraban, L.; Harazim, S. M.; Sanchez, S.; Schmidt, O. G. Chemotactic Behavior of Catalytic Motors in Microfluidic Channels. *Angew. Chem., Int. Ed.* **2013**, *52*, 5552–5556.
66. Capson, T. L.; Peliska, J. A.; Kaboord, B. F.; Frey, M. W.; Lively, C.; Dahlberg, M.; Benkovic, S. J. Kinetic Characterization of the Polymerase and Exonuclease Activities of the Gene 43 Protein of Bacteriophage T4. *Biochemistry* **1992**, *31*, 10984–10994.
67. Astumian, R. D. Stochastic Conformational Pumping: a Mechanism for Free-Energy Transduction by Molecules. *Annu. Rev. Biophys.* **2011**, *40*, 289–313.
68. Astumian, R. D. Thermodynamics and Kinetics of a Brownian Motor. *Science* **1997**, *276*, 917–922.
69. Reimann, P. Brownian Motors: Noisy Transport Far from Equilibrium. *Phys. Rep.* **2002**, *361*, 57–265.
70. Astumian, R. D. Making Molecules into Motors. *Sci. Am.* **2001**, *285*, 56–64.
71. Sengupta, S.; Patra, D.; Ortiz-Rivera, I.; Agrawal, A.; Shklyaev, S.; Dey, K. K.; Córdova-Figueroa, U.; Mallouk, T. E.; Sen, A. Self-Powered Enzyme Micropumps. *Nat. Chem.*, in press. DOI: 10.1038/NCHEM.1895.
72. Prieve, D. C.; Anderson, J. L.; Ebel, J. L.; Lowell, M. E. Motion of a Particle Generated by Chemical Gradients. Part 2. Electrolytes. *J. Fluid Mech.* **1984**, *148*, 247–269.
73. Sokolov, A.; Aranson, I. S. Reduction of Viscosity in Suspension of Swimming Bacteria. *Phys. Rev. Lett.* **2009**, *103*, 148101.
74. Liu, R.; Sen, A. Autonomous Nanomotor Based on Copper–Platinum Segmented Nanobattery. *J. Am. Chem. Soc.* **2011**, *133*, 20064–20067.
75. Wang, W.; Chiang, T.-Y.; Velegol, D.; Mallouk, T. E. Understanding the Efficiency of Autonomous Nano- and Microscale Motors. *J. Am. Chem. Soc.* **2013**, *135*, 10557–10565.
76. Chang, S. T.; Paunov, V. N.; Petsev, D. N.; Velev, O. D. Remotely Powered Self-Propelling Particles and Micropumps Based on Miniature Diodes. *Nat. Mater.* **2007**, *6*, 235–240.
77. Rush, J.; Konigsberg, W. H. Rapid Purification of Overexpressed T4 DNA Polymerase. *Prep. Biochem.* **1989**, *19*, 329–340.
78. Xia, Y.; Whitesides, G. M. Soft Lithography. *Annu. Rev. Mater. Sci.* **1998**, *28*, 153–184.
79. Miranda, O. R.; Chen, H. T.; You, C. C.; Mortenson, D. E.; Yang, X. C.; Bunz, U. H. F.; Rotello, V. M. Enzyme-Amplified Array Sensing of Proteins in Solution and in Biofluids. *J. Am. Chem. Soc.* **2010**, *132*, 5285–5289.